Magnetosonic Mach number dependence of the efficiency of reconnection between planetary and interplanetary magnetic fields

A. Grocott,[1] S. V. Badman,[1] S. W. H. Cowley,[1] S. E. Milan,[1] J. D. Nichols,[1] and T. K. Yeoman[1]

Received 3 April 2009; revised 20 May 2009; accepted 26 May 2009; published 18 July 2009.

[1] We present a statistical investigation into the magnetosonic Mach number dependence of the efficiency of reconnection at the Earth's dayside magnetopause. We use the transpolar voltage V_{PC}, derived from radar observations of the ionospheric electric field, as a proxy for the dayside reconnection voltage. Our results show that the IMF clock angle dependence of V_{PC} is closely approximated by the function $f(\theta) = \sin^2(\theta/2)$, which we use in the derivation of a solar wind transfer function $E^* = E_{SW} f(\theta)$, wherein E_{SW} is the solar wind electric field. We find that V_{PC} is strongly related to E^*, increasing almost linearly with small E^* but saturating as E^* becomes high. We also find that E^* is strongly dependent on the magnetosonic Mach number, M_{MS}, decreasing to near-zero values as M_{MS} approaches 12, due principally to decreasing values of the IMF strength. V_{PC}, on the other hand, is only weakly related to M_{MS} and, for lower, more usual values of E^*, actually shows a modest increase with increasing M_{MS}. This result has implications for the solar wind-magnetosphere interaction at the outer planets where the Mach number is typically much higher than it is at 1 AU. Examples of SuperDARN convection maps from two high Mach number intervals are also presented, illustrating the existence of fairly typical reconnection driven flows. We thus find no evidence for a significant reduction in the magnetopause reconnection rate associated with high magnetosonic Mach numbers.

Citation: Grocott, A., S. V. Badman, S. W. H. Cowley, S. E. Milan, J. D. Nichols, and T. K. Yeoman (2009), Magnetosonic Mach number dependence of the efficiency of reconnection between planetary and interplanetary magnetic fields, *J. Geophys. Res.*, *114*, A07219, doi:10.1029/2009JA014330.

1. Introduction

[2] The dynamics of planetary magnetospheres are fundamentally determined by two physical processes. One is the rotation of the planet, which drives circulation of plasma in the magnetosphere via frictional coupling with its atmosphere. The other is magnetic reconnection between the magnetospheric field and the interplanetary magnetic field (IMF), which enables the transport of plasma across the magnetopause and couples solar wind energy and momentum into the system. While it has long been understood that the Earth's magnetosphere is predominantly solar wind driven [e.g., *Dungey*, 1961; *Cowley et al.*, 2003], theoretical and observational evidence suggests that it is the rapid planetary rotation of the gas giants that is dominant in governing the dynamics of their magnetospheres [e.g., *Brice and Ioannidis*, 1970; *Hill*, 1979; *Siscoe and Summers*, 1981; *Hill et al.*, 1983]. However, recent studies have suggested that solar wind coupling may also play a significant role [e.g., *Khurana*, 2001; *Badman et al.*, 2005; *Nichols et al.*, 2006; *Badman and Cowley*, 2007; *McAndrews et al.*, 2008], which is thus important to quantify and understand.

[3] Studies at Earth have shown that the magnetic flux that can be transferred via solar wind coupling is largely governed by the strength and direction of the IMF. Early studies of geomagnetic indices revealed that geomagnetic activity is greatest when the IMF is directed southward [*Fairfield and Cahill*, 1966; *Rostoker and Fälthammar*, 1967], although more complex empirical transfer functions have since been derived [e.g., *Wygant et al.*, 1983]. One such widely used function takes the form of the solar wind electric field, $v_{SW}B_\perp$ (where v_{SW} is the solar wind speed and $B_\perp$ is the IMF vector component perpendicular to the direction of the solar wind flow), multiplied by an IMF clock angle function, $f(\theta)$, (where θ is the IMF clock angle, measured from north). This clock angle dependence is often chosen to have the form $f(\theta) = \sin^n(\theta/2)$, where n is an integer usually equal to either 2 or 4 [*Perreault and Akasofu*, 1978; *Kan and Lee*, 1979], and will be discussed further in section 2.3, below. The dayside reconnection rate is then estimated by multiplying this electric field by a characteristic scale length, suggested by *Milan* [2004] to be of the order of 5–8 R_E. This concept has been used in a

[1]Department of Physics and Astronomy, University of Leicester, Leicester, UK.

0148-0227/09/2009JA014330

number of studies of the solar wind interaction with the Earth's magnetosphere [e.g., *Hubert et al.*, 2006; *Milan et al.*, 2007] and has since been adapted for use at Saturn by *Jackman et al.* [2004] and at Jupiter by *Nichols et al.* [2006] and has been used to quantify and discuss the solar wind interaction at these planets by *Badman and Cowley* [2007].

[4] Despite these results, the extent to which magnetopause reconnection can influence the dynamics of the outer planets is still widely debated. One argument for it having very little influence stems from the suggestion that the efficiency of reconnection is strongly governed by the magnetosonic Mach number [*Russell et al.*, 2008], which is typically 10 at the orbit of Saturn compared to 6 at 1 AU [*Russell et al.*, 1990]. *Scurry and Russell* [1991] studied the efficiency of the reconnection mechanism at Earth using the Am geomagnetic index [*Mayaud*, 1980] as a proxy for energy transfer into the Earth's magnetosphere and found that their empirically determined reconnection efficiency factor based on Am drops to zero for Mach numbers larger than 7. This result suggests that any transfer function derived under usual conditions at Earth would be invalid at the outer planets.

[5] In a more direct approach to studying the reconnection mechanism, *Kuo et al.* [1995] and *Russell et al.* [1996] conducted studies of flux transfer events (FTEs) using magnetic field data from the International Sun-Earth Explorer-1/-2 (ISEE) satellites and found that FTE occurrence decreases with increasing solar wind magnetosonic Mach number. On the other hand, *Wang et al.* [2006] studied FTE statistics using Cluster data and found that the FTE occurrence rate generally increases with increasing solar wind magnetosonic Mach number. Only beyond a Mach number of $\sim$8.5 did the occurrence show a significant decrease, at which point their IMF and FTE distributions were close to zero. Their results also revealed a slight general increase of FTE separation time with increasing magnetosonic Mach number, but no strong dependence of FTE peak-peak magnitude.

[6] While the FTE studies discussed above provide a direct measure of individual reconnection events, they do not provide a full quantification of the reconnection process owing to the localized nature of the spacecraft observations. Even multispacecraft investigations are unable to routinely determine the azimuthal extent of FTEs which may be more than 10,000 km [*Fear et al.*, 2008]. The studies using geomagnetic indices, on the other hand, do provide a more global view of the energy throughput of the magnetosphere. However, they provide a far from direct measure of the reconnection rate, or of the flux throughput of the magnetosphere in particular, because their response to enhanced convection is dependent on the ionospheric Hall conductivity. *Kamide and Richmond* [1982] found that estimates of the ionospheric electric field obtained using geomagnetic data as a proxy depend strongly upon the ionospheric conductivity and are thus less reliable than the electric fields and flows observed more directly by satellites and radar techniques. Indeed, *Grocott et al.* [2003, 2004, 2008] found intervals in which dayside reconnection persisted for many hours under northward, but B_Y dominated IMF conditions, without exciting any significant perturbations in the ground magnetic field that would be evident in geomagnetic indices.

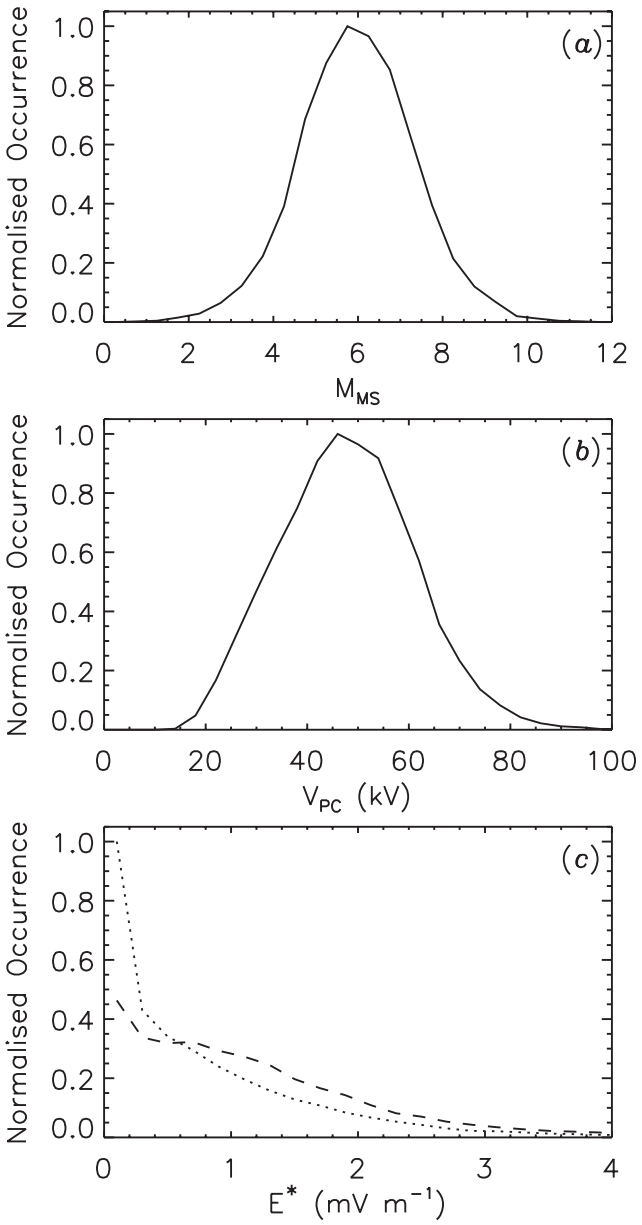

Figure 1. The distributions of (a) magnetosonic Mach number M_{MS}, (b) ionospheric transpolar voltage V_{PC}, and (c) the transfer function E^*. The dashed and dotted lines in Figure 1c correspond to $n = 2$ and $n = 4$, respectively, in the determination of E^* from equation (4).

[7] In this paper we use total ionospheric transpolar voltage data, derived from radar measurements of the ionospheric flow, as a more direct measure of the global flux throughput of the magnetosphere. Over suitably long timescales, and in the absence of other significant drivers, the transpolar voltage is equal to the dayside (and nightside) reconnection rate. We therefore use two hour averages of transpolar voltage data as a proxy for the dayside reconnection rate, which we investigate for different magnetosonic Mach number regimes. Our results, from both statistical analyses and case studies, show that the transpolar voltage exhibits no strong variation with the magnetosonic Mach number and, in particular, no significant downturn for

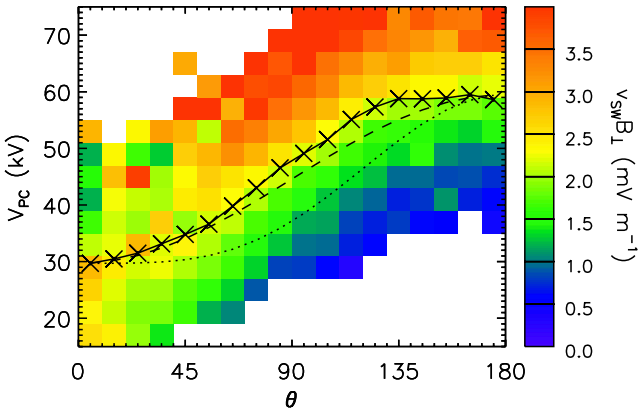

Figure 2. The transpolar voltage V_{PC}, versus IMF clock angle θ in bins of 4 kV $\times$ 10°. Each bin is color coded to the corresponding mean value of $v_{SW}B_{\perp}$ according to the color bar on the right. The mean V_{PC} in each clock angle bin is also indicated (crosses on solid curve) with $\sin^2(\theta/2)$ (dashed line) and $\sin^4(\theta/2)$ (dotted line) functional forms superposed.

Mach numbers exceeding 7 as suggested by *Scurry and Russell* [1991].

2. Data Analysis

[8] Data from two sources spanning the 8 year interval 1999–2006 are used in this study: upstream interplanetary data from the Advanced Composition Explorer (ACE) spacecraft [*Stone et al.*, 1998] and ionospheric electric field data from the northern hemisphere Super Dual Auroral Radar Network (SuperDARN [*Greenwald et al.*, 1995]). SuperDARN provides a map of high-latitude ionospheric convection every 2 minutes, from which we can derive the ionospheric transpolar voltage (see section 2.2). The ACE Solar Wind Electron Proton Alpha Monitor (SWEPAM [*McComas et al.*, 1998]) provides measurements of the proton speed, temperature and number density at 64 s resolution and the Magnetic Field Experiment (MFE [*Smith et al.*, 1998]) provides measurements of the IMF at 16 s resolution. Throughout this paper the IMF data are presented and discussed in terms of their geocentric solar magnetospheric (GSM) coordinates. These data have been time-lagged to the dayside ionosphere using the method by *Khan and Cowley* [1999]. This technique involves calculating the propagation delay of field changes from ACE to the dayside ionosphere and includes the propagation time in the solar wind upstream of the bow shock, the frozen-in transit time across the subsolar magnetosheath, and the Alfvénic propagation time along open field lines from the subsolar magnetopause to the ionosphere. Both the SuperDARN and ACE data sets have then been averaged to a time resolution of 2 hours to remove fluctuations occurring on shorter timescales and better approximate a "steady state" response of the ionosphere to the solar wind. The imposition of further constraints on IMF and solar wind variability within each 2 hour bin (e.g., standard deviation thresholds) was also investigated but was found to have little effect on the results. We have, however, imposed a data coverage constraint on the radar data to ensure reliable determination of the transpolar voltage, discussed in more detail below. Both data sets have nevertheless been kept coincident so that any intervals removed from one set have also been removed from the other.

[9] The data set that results from this analysis consists of almost 20,000 2-hour intervals from which to derive our statistics. The specific parameters required for this study are the magnetosonic Mach number, M_{MS}, the solar wind transfer function, E^*, and the ionospheric transpolar voltage, V_{PC}. In the following sections we briefly describe the derivation of each, and their distributions, which are shown in Figure 1.

2.1. Magnetosonic Mach Number

[10] The magnetosonic Mach number, M_{MS}, is given by

$$M_{MS} = \frac{v_{SW}}{\sqrt{{v_A}^2 + {v_S}^2}}, \quad (1)$$

where v_A is the Alfvén speed, $B/\sqrt{\mu_0\rho}$, and v_S is the sound speed, $\sqrt{\gamma P/\rho}$. In each expression the solar wind mass density, ρ, is derived assuming an alpha particle to proton ratio of 4%. In the calculation of the sound speed, the ratio of specific heats, γ, is taken to be 5/3 and the thermal pressure, P, is given by $n_p k(T_i + T_e)$. Although T_i is routinely available in the ACE data set, T_e is not. However, according to *Newbury et al.* [1998] the solar wind electron temperature is relatively constant compared to the proton temperature, and is not influenced by other concurrent parameters in the solar wind. We have therefore used their best fixed estimate of $T_e = 1.41 \times 10^5$ K in our calculation of the pressure. The distribution of M_{MS} is shown in Figure 1a, which reveals an approximately Gaussian distribution ranging from ~1 to 12, with a peak at ~6, in good agreement with the expected value at 1 AU [e.g., *Russell et al.*, 1990].

2.2. Ionospheric Transpolar Voltage

[11] The ionospheric transpolar voltage, V_{PC}, is derived using the SuperDARN global convection analysis technique of *Ruohoniemi and Baker* [1998] (hereafter referred to as the Map Potential technique). This technique involves mapping the line-of-sight radar velocity measurements onto a polar grid, and using them to determine a solution for the electrostatic potential, which is expressed in spherical harmonics. Information from the statistical model of *Ruohoniemi and Greenwald* [1996], parameterized by concurrent IMF conditions, is used to stabilise the solution where no measurements are available. However, we have imposed a condition that there must be at least 200 radar velocity measurements in any one 2-min map for it to be included in our analysis, which serves to minimize any influence of the statistical model in the results. We have also used fits only up to a relatively low sixth order in the spherical harmonic expansion. As we are only interested in a global measure of the convection, which derives little benefit from using higher orders, this also serves to constrain the effects of regions of poor data coverage. Calculation of the total transpolar voltage then simply involves taking the difference between the maximum and minimum values in the potential map, i.e.

$$V_{PC} = \Phi_{\max} - \Phi_{\min}, \quad (2)$$

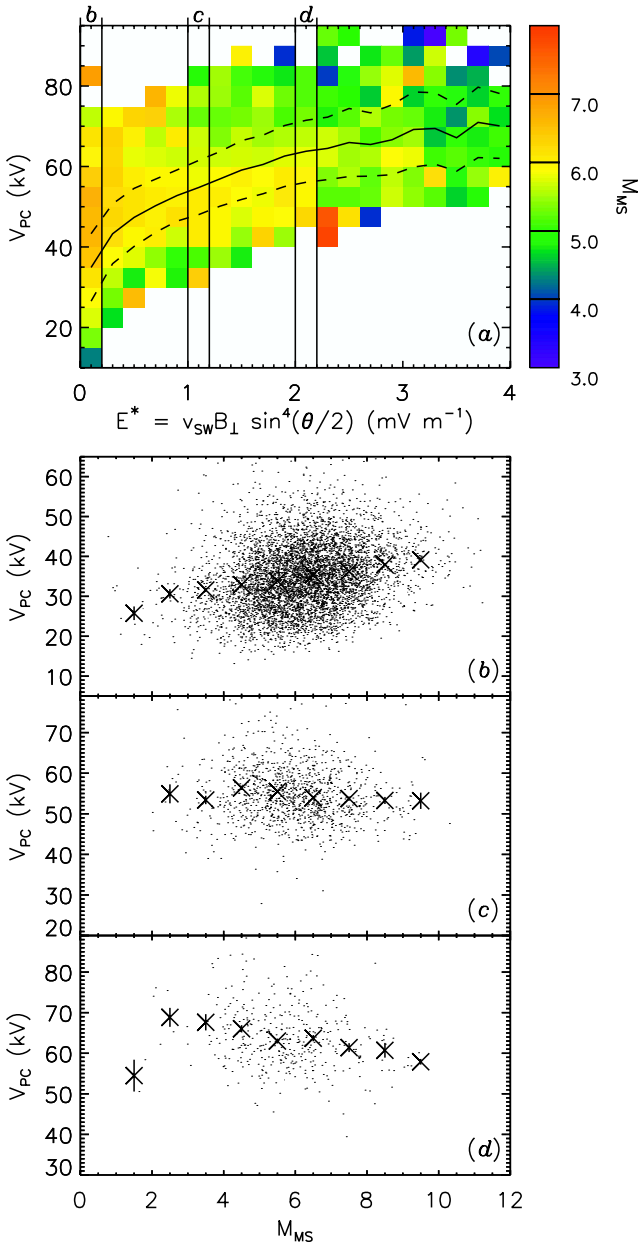

Figure 3. (a) V_{PC} versus $E^* = v_{SW}B_\perp \sin^4(\theta/2)$ in bins of 5 kV × 0.2 mV m^{-1}, color coded to the mean value of M_{MS} in each bin according to the color bar on the right. The mean V_{PC} in each E^* bin is also indicated (solid curve) with ±1 standard deviation from this mean also shown (dashed curves). The columns indicated by the labels (b–d) are then expanded in the lower three panels which show V_{PC} versus M_{MS} for the corresponding E^* ranges (black dots). Mean values of V_{PC} in 1-unit wide bins of M_{MS} are superposed with ±1 standard error indicated on each mean by the short vertical bars.

where Φ is related to the convection electric field and velocity by the familiar

$$\mathbf{E} = -\nabla\Phi;\ \mathbf{v} = \frac{\mathbf{E}\times\mathbf{B}}{B^2}. \quad (3)$$

The transpolar voltage, V_{PC}, should then be a very good proxy for the reconnection rate if we assume that the dayside and nightside reconnection rates are approximately equal over the 2-hour averages used in this study. The distribution of V_{PC}, shown in Figure 1b, also has a Gaussian distribution, ranging from ~15 to 95 kV with a peak at ~50 kV. This lower limit of ~15 kV may be related to a combination of viscous coupling [*Milan*, 2004] or some minimum level reconnection that is independent of the IMF [*Farrugia et al.*, 2007].

2.3. Solar Wind Transfer Function

[12] We have derived a solar wind transfer function

$$E^* = v_{SW}B_\perp \sin^n(\theta/2), \quad (4)$$

which is equal to the solar wind electric field ($v_{SW}B_\perp$), multiplied by an IMF clock angle function ($\sin^n(\theta/2)$), as discussed above. Here v_{SW} is simply the proton bulk speed, as measured by the SWEPAM instrument, and is taken to be directed radially away from the Sun. $B_\perp$ is the IMF vector component perpendicular to v_{SW}, and is taken to be equal to $\sqrt{B_Y^2 + B_Z^2}$. θ is the IMF clock angle, which is equal to the angle between the $B_\perp$ vector and the GSM z direction. An integer, n, governs the strength of the angular dependence and will be discussed further in section 3.1, below. The distribution of E^*, shown in Figure 1c for values of $n = 2$ (dashed line) and $n = 4$ (dotted line), decreases with increasing E^*, having a somewhat more even distribution for $n = 2$. In both cases, over 80% of E^* values fall below 2 mV m^{-1}.

3. Statistical Analysis

3.1. Clock Angle Dependence of V_{PC}

[13] As discussed in section 1, we will be using the transpolar voltage as a proxy for the reconnection rate at the dayside magnetopause and, in order to account for the clock angle dependence of the reconnection efficiency, we include a function of θ in equation (4). Before we investigate any additional dependencies of V_{PC}, however, we briefly examine what the θ dependence actually is. We have therefore averaged our V_{PC} data set in 10° wide bins of IMF clock angle, shown in Figure 2 by the crosses and solid curve, and compared the resulting trend to given functions of θ. Although the standard errors of the mean V_{PC} values are small (so much so that they are not representable in Figure 2) there is nevertheless some spread in V_{PC} within each θ bin. This spread is indicated on Figure 2 by the range of V_{PC} covered by the colored rectangles. Each rectangle represents a 4 kV subdivision of each 10° clock angle bin, which has then been color coded to the mean value of the solar wind electric field, $v_{SW}B_\perp$, according to the color bar on the right. For $\theta > 60°$ V_{PC} is well ordered by $v_{SW}B_\perp$, such that higher voltages correspond to higher values of $v_{SW}B_\perp$. For smaller values of θ (more northward IMF) the relationship between V_{PC} and $v_{SW}B_\perp$ is less clear, such that larger V_{PC} are not associated with larger $v_{SW}B_\perp$. To ensure that this trend is not strongly influenced by extremes of solar wind velocity or total IMF strength we have compared this result to that obtained using a subset of V_{PC} corresponding to the more typical ranges of solar wind

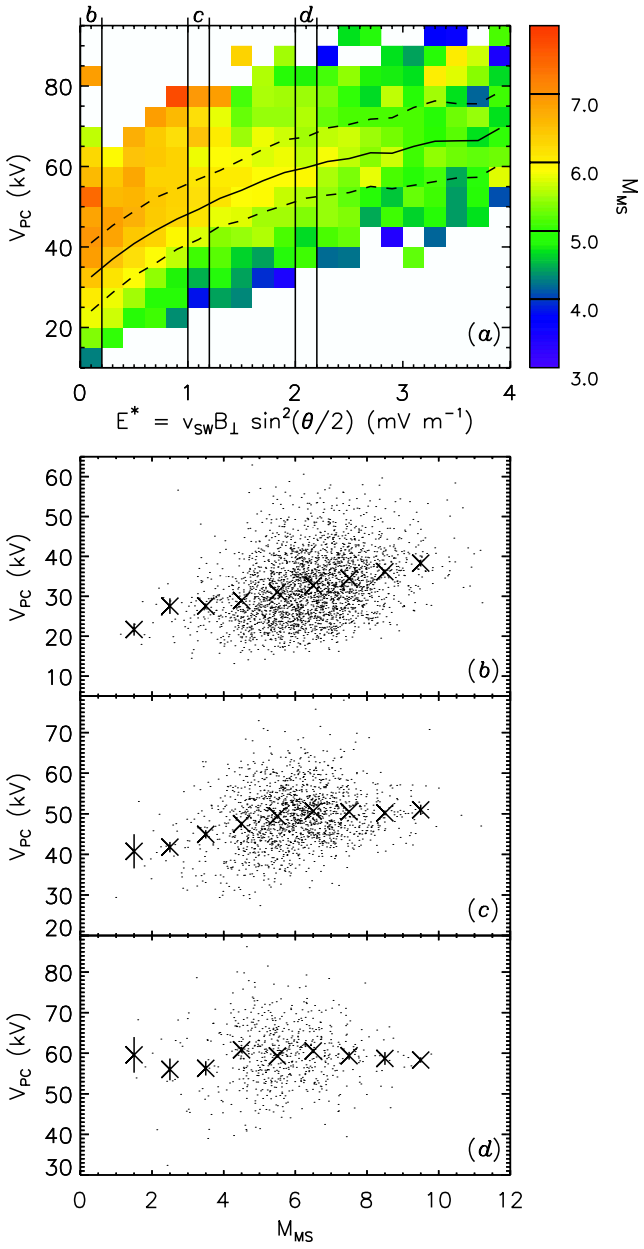

Figure 4. As in Figure 3, but for the case $E^* = v_{SW}B_\perp \sin^2(\theta/2)$.

speed and magnetic field strength as determined by the full width at half maximum of the distributions of each. This reduced data set (not shown) produces a trend which is almost identical, except for the expected reduction in the range of $v_{SW}B_\perp$.

[14] The dotted and dashed curves superposed on Figure 2 illustrate $\sin^4(\theta/2)$ and $\sin^2(\theta/2)$ functions, respectively, adjusted in amplitude and offset to best fit the mean V_{PC} curve in each case. It is immediately evident that $\sin^4(\theta/2)$ does not adequately represent the clock angle dependence of V_{PC}. The function rises too slowly with increasing clock angle at small values, and then too sharply at higher values. While this might be appropriate for modeling the clock angle dependence of geomagnetic indices (for reasons discussed in section 1) it is clear that the $\sin^2(\theta/2)$ dependence provides a better fit to V_{PC} in this case. In fact, this curve does not precisely follow the shape of the V_{PC} curve either, suggesting that a different fit altogether might be appropriate. However, as will be shown below, $\sin^2(\theta/2)$ produces a significantly better ordering of V_{PC} with respect to E^* than $\sin^4(\theta/2)$, whereas a rudimentary investigation into the use of other,

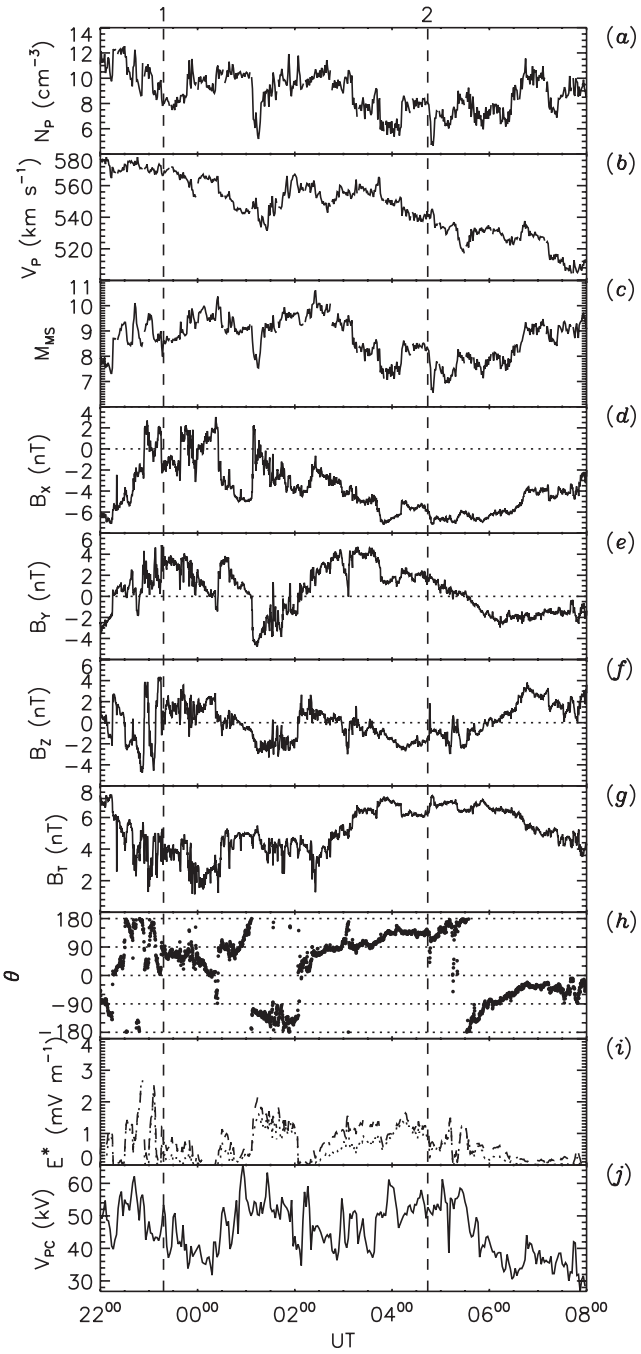

Figure 5. Time series data from 14/15 February 2000 showing (a) the solar wind number density, (b) the solar wind speed, (c) the magnetosonic Mach number, (d–f) the three IMF GSM components, (g) the IMF strength, (h) the IMF clock angle, (i) the transfer function E^* (dashed line for $n = 2$, dotted line for $n = 4$), and (j) the ionospheric transpolar voltage. The two vertical dashed lines indicate times of the two convection maps in Figure 6.

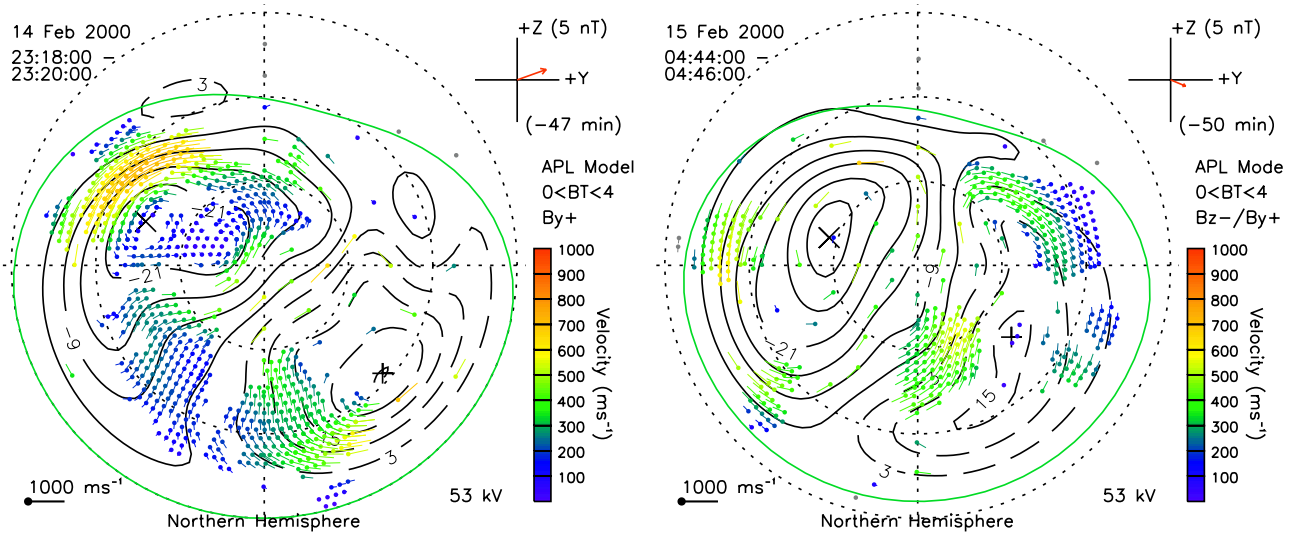

Figure 6. Streamlines and vectors of the northern hemisphere ionospheric flow, derived from SuperDARN velocity measurements using the map potential algorithm, are shown on a geomagnetic grid from 60° to the pole, with (top) noon and (left) dusk. The intervals displayed are (left) 23:18–23:20 UT and (right) 04:44–04:46 UT on 14/15 February 2000. Indicated in the bottom right-hand corner of each map is the total transpolar voltage V_{PC}. In the top right-hand corner, we indicate the direction and magnitude (in the Y–Z plane) of the IMF and the flow model employed to stabilize the potential solution in regions where no data are available, obtained from the statistical study of *Ruohoniemi and Greenwald* [1996].

more elaborate, clock angle functions reveals no further discernible improvement. In the following sections we will show results using estimates of E^* determined with both $f(\theta) = \sin^2(\theta/2)$ and $f(\theta) = \sin^4(\theta/2)$ in order to illustrate the significance of $f(\theta)$ on our results.

3.2. M_{MS} Dependence

[15] Figures 3 and 4 show the relationship between the V_{PC}, E^*, and M_{MS} parameters discussed in section 2. In Figure 3, E^* has been estimated using $n = 4$ in equation (4) and in Figure 4, using $n = 2$. In both cases (a) shows V_{PC} versus E^* in bins of 5 kV × 0.2 mV m^{-1}, color coded to the mean value of M_{MS} in each bin, according to the color bar on the right. The mean V_{PC} in each E^* bin is also indicated (solid curve) with ±1 standard deviation from this mean also shown (dashed curves). The columns indicated by the labels (b–d) are then expanded in the lower three panels which show V_{PC} versus M_{MS} for the corresponding E^* bins (black dots). Bins at the lower end of the E^* distribution have been chosen because they are the most populous (see Figure 1c). Mean values of V_{PC}, in 1-unit wide bins of M_{MS}, are also shown by crosses in (b–d), with ±1 standard error indicated on each mean by the short vertical bars.

[16] Looking first at Figure 3a we see a clear dependence of V_{PC} on E^* such that, in general, higher transpolar voltages are related to higher values of E^*. The gradient of the mean V_{PC} (solid curve) is noticeably highest for low values of E^*, dropping rapidly with increasing E^*. This results in there being ~20 kV variation in averaged V_{PC} over the solar wind electric field range $0 < E^* < 1$ mV m^{-1} with a further ~20 kV variation over the range $1 < E^* < 4$ mV m^{-1}. While there is a known tendency of the transpolar voltage to saturate for high values of E^* [*Russell et al.*, 2001; *Shepherd et al.*, 2003] these results imply that the relationship between V_{PC} and E^* with $n = 4$ is not very linear, as assumed by *Jackman et al.* [2004] and *Nichols et al.* [2006], particularly at the more usual end of the E^* range. If we now consider the behavior of M_{MS} we see that higher M_{MS} values are associated with lower E^*, as a result of the dependency of both on the IMF strength. Any relationship between V_{PC} and M_{MS}, however, is marginal at best. It becomes somewhat clearer if we consider fixed E^* bins as shown in (b–d) which suggest that for low E^*, shown in (b), V_{PC} is weakly correlated with M_{MS} whereas for higher E^*, shown in (d), V_{PC} is weakly anticorrelated with M_{MS}.

[17] Figure 4 shows the same analysis as Figure 3 but for E^* estimated using $n = 2$ in equation (4). The relationship between V_{PC} and E^* is more linear in this case, especially at low E^*, although there is perhaps slightly more spread in the data. However, the Mach number dependence shown in (a) is now much more pronounced, with a very clear ordering both with respect to E^* and V_{PC}, especially for the $0 < E^* < 2$ mV m^{-1} regime. This is again evidenced further by considering (b–d). Both (b) and (c) now show a general tendency for higher voltages to be driven at higher Mach numbers for a given E^*. While (d) now shows no clear dependency there is certainly no discernible evidence for a downturn in V_{PC} at high M_{MS}. While it may be true, therefore, that for unusually high solar wind electric fields a high magnetosonic Mach number will cause the ionospheric transpolar voltage to saturate at a lower value, this effect is small. There is certainly no evidence for a threshold of M_{MS} beyond which V_{PC} drops to significantly lower values, for any E^* regime. For lower, more usual, values of E^* it in fact

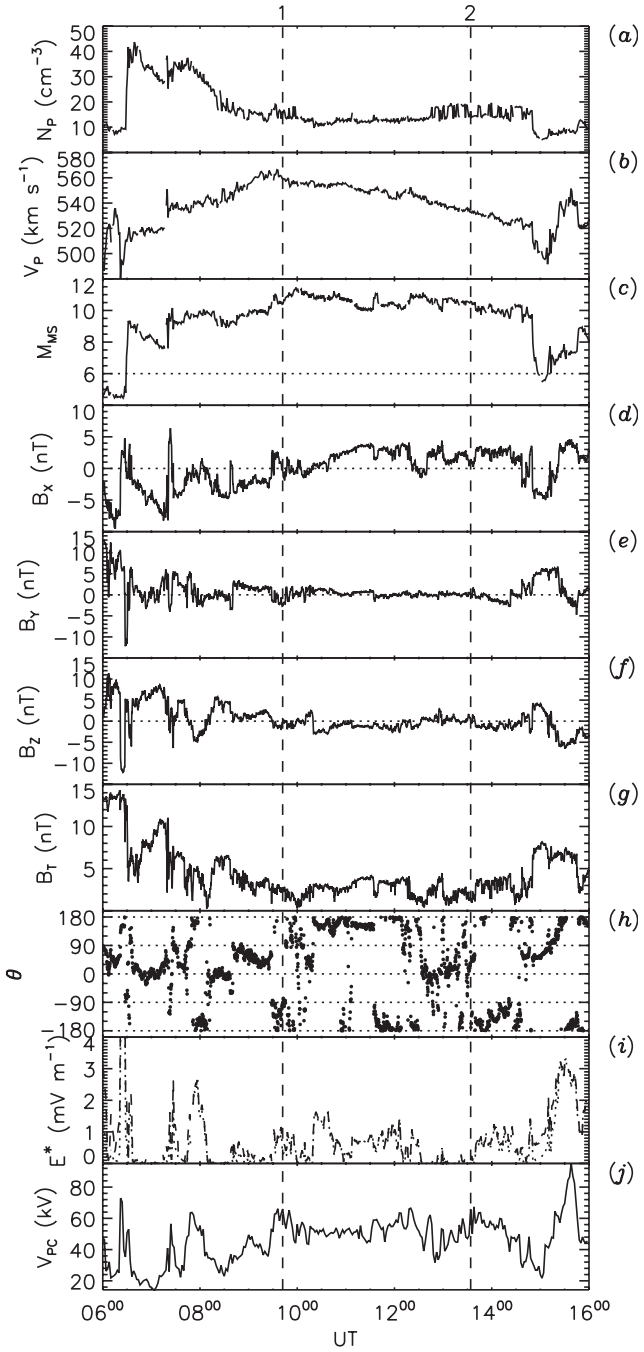

Figure 7. Time series data from 30 December 2004 in the same format as Figure 5.

appears to be the case that, for a given range of E^*, the highest ionospheric transpolar voltages are driven when the Mach number is high. Of course, the very highest voltages do tend to be associated with lower values of M_{MS}, but this appears to be due to the intrinsic anticorrelation between M_{MS} and E^* rather than some limit on the reconnection that can be driven by a high Mach number solar wind.

4. Case Study Examples

[18] In the previous section we have shown that a high solar wind magnetosonic Mach number does not appear to prohibit significant magnetosphere-solar wind coupling. In this section we investigate exactly what form the convection driven under such conditions might take by considering exemplar interplanetary and ionospheric data from two high M_{MS} intervals. Figure 5 presents time series data from the first of the two intervals, 22:00 UT on 14 February–08:00 UT on 15 February 2001, consisting of (a) the solar wind number density, (b) the solar wind speed, (c) the magnetosonic Mach number, (d–f) the three IMF GSM components, (g) the IMF strength, (h) the IMF clock angle, (i) the solar wind transfer function E^* (dashed line for $n = 2$, dotted line for $n = 4$), and (j) the ionospheric transpolar voltage. The two vertical dashed lines correspond to times from which we show representative ionospheric convection patterns, discussed below. Looking at (c) we can see that the magnetosonic Mach number was greater than 7 for the whole interval, rising to between 9 and 10 for the first ~4 hours. Looking at (b) and (g) we can see that this was largely due to an elevated solar wind speed and concurrent decrease in the total magnetic field strength. During this time, as shown in (h), the IMF clock angle varied considerably, leading to the variations in E^* shown in (i). V_{PC}, shown in (j), peaked at ~60 kV and remained above 40 kV for much of the interval, only dropping to lower values when E^* went close to zero. This provides strong evidence for the persistence of dayside reconnection throughout this high Mach number interval, modulated by variations in the IMF clock angle. Importantly, it shows that the enhancements in E^* are generally accompanied by enhancements in V_{PC} throughout the interval, irrespective of the magnitude of M_{MS}.

[19] In Figure 6 we show example convection patterns, from the times indicated in Figure 5 by the vertical dashed lines, to give an impression of the nature of the convection during the interval. Two maps are shown, containing data from 23:18–23:20 UT and 04:44–04:46 UT, which consist of fitted radar velocity vectors, and streamlines of the ionospheric electric potential, as discussed in section 2.2 above. In the first map we show the convection from the earlier, higher Mach number part of the interval, and we see a fairly unremarkable twin-cell convection pattern, with flows of up to ~700 m s^{-1} and a transpolar voltage of over 50 kV. In the second map we show the convection from later in the interval when the Mach number had subsided somewhat. Although in this case the data coverage is to some extent reduced, there is still evidence of a similar flow pattern, with the same transpolar voltage. It would appear therefore that, irrespective of Mach number, there is evidence for ongoing dayside driving in both cases.

[20] In Figures 7 and 8 we show time series data and convection maps, respectively, from a second interval, on 30 December 2004. In this case the Mach number remained consistently high for longer than in the previous example, with $M_{MS} > 10$ for over 4 hours from ~10:00 to 14:00 UT. During these 4 hours the total magnetic field strength remained low (~3 nT), while V_{PC} was consistently of the order ~50 kV. In this case, periods of low E^* appear to imply an underestimate of the voltage when compared to higher values earlier on in the interval. For example, consider the situation at ~08:00 UT, where $E^* \approx 2$ mV m^{-1} and $M_{MS} \approx 10$, and then at ~10:00 UT, where $E^* \approx 1$ mV m^{-1} and $M_{MS} \approx 12$. In both cases V_{PC} peaks at

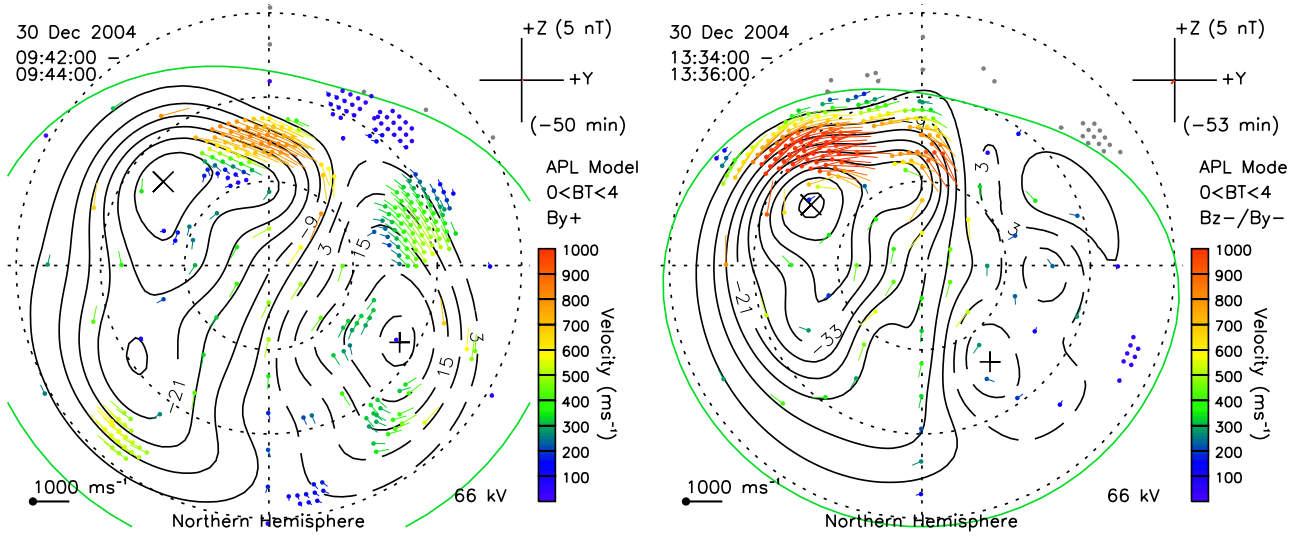

Figure 8. Streamlines and vectors of the northern hemisphere ionospheric flow from (left) 09:42–09:44 UT and (right) 13:34–13:36 UT on 30 December 2004 in the same format as Figure 6.

~60 kV, suggesting that the higher M_{MS} corresponds to an increased reconnection efficiency such that a quasiconstant V_{PC} is maintained despite the drop in E^*. Turning to the convection maps, they show fast flows in the noon-sector ionosphere suggesting again that magnetopause reconnection was ongoing. Both this interval, and the previous one, exhibit nothing to suggest that reconnection is not playing a dominant role in driving convection despite the continuing high solar wind magnetosonic Mach number.

5. Summary

[21] It has recently been suggested that reconnection is unlikely to play a dominant role in driving circulation of the magnetospheres of the outer planets owing to an inefficiency of reconnection when the magnetosonic Mach number is high [*Russell et al.*, 2008]. Previous studies of energy transfer into the magnetosphere, such as that conducted by *Scurry and Russell* [1991], used geomagnetic indices as a proxy for the dayside reconnection efficiency which was found to tend to zero for high solar wind magnetosonic Mach numbers. However, it has been shown previously that dayside reconnection can persist for many hours at a modest level, for example, during intervals of northward, but B_Y-dominated IMF, without exciting significant perturbations in the ground magnetic field that would be evident in geomagnetic indices [e.g., *Grocott et al.*, 2003]. This suggests that these indices may be less reliable as a proxy for the reconnection rate than more direct satellite or radar techniques. We have therefore used the transpolar voltage, V_{PC}, derived from ionospheric radar measurements, as a proxy for the reconnection rate and have investigated whether the relationship between V_{PC} and $E^* = v_{SW}B_{\perp}\sin^n(\theta/2)$ changes for different Mach number regimes.

[22] Our results show that the IMF clock angle dependence of V_{PC} is closely approximated by the function $f(\theta) = \sin^2(\theta/2)$. They also show that, although V_{PC} tends to saturate at smaller values when M_{MS} is high, this is more likely to result from the strong relationship between E^* and M_{MS} than any direct influence of M_{MS} on V_{PC}. This we have illustrated by considering the relationship between V_{PC} and M_{MS} for fixed ranges of E^* and we have found that, for more usual vales of E^* (below ~2 mV m^{-1}), V_{PC} actually increases with increasing M_{MS}. This implies that, while a low E^* will inherently result in a lower V_{PC}, the reconnection mechanism may become more efficient at high Mach numbers such that significant magnetospheric circulation can continue to be driven. We have also shown example SuperDARN convection maps from two high Mach number intervals which illustrate the existence of fairly typical reconnection driven flows and thus reveal no evidence for a significant reduction in the reconnection rate associated with high Mach numbers.

[23] **Acknowledgments.** We thank the PIs of the SuperDARN radars for provision of the radar data and R.J. Barnes of the Johns Hopkins University for the "Map-Potential" algorithm. We also thank the ACE MAG and SWEPAM instrument teams and the ACE Science Center for providing the ACE data. A.G., S.V.B., and J.D.N. were supported during this study by STFC grant PP/E000983/1. SuperDARN operations at the University of Leicester are supported by STFC grant PP/E007929/1.

[24] Amitava Bhattacharjee thanks Charles Farrugia and Lorenzo Trenchi for their assistance in evaluating this paper.

References

Badman, S. V., and S. W. H. Cowley (2007), Significance of Dungey-cycle flows in Jupiter's and Saturn's magnetospheres, and their identification on closed equatorial field lines, *Ann. Geophys.*, *25*, 941–951.

Badman, S. V., E. J. Bunce, J. T. Clarke, S. W. H. Cowley, J.-C. Gérard, D. Grodent, and S. E. Milan (2005), Open flux estimates in Saturn's magnetosphere during the January 2004 Cassini-HST campaign, and implications for reconnection rates, *J. Geophys. Res.*, *110*(A9), A11216, doi:10.1029/2005JA011240.

Brice, N. M., and G. A. Ioannidis (1970), The magnetospheres of Jupiter and Earth, *Icarus*, *13*, 173, doi:10.1016/0019-1035(70)90048-5.

Cowley, S. W. H., et al. (2003), Solar-wind-magnetosphere-ionosphere interactions in the Earth's plasma environment, *Philos. Trans. A.*, *361*, 113–126.

Dungey, J. W. (1961), Interplanetary magnetic field and the auroral zones, *Phys. Rev. Lett.*, *6*, 47–48, doi:10.1103/PhysRevLett.6.47.

Fairfield, D. H., and L. J. Cahill Jr. (1966), Transition region magnetic field and polar magnetic disturbances, *J. Geophys. Res.*, *71*, 155–169.

Farrugia, C. J., A. Grocott, P. E. Sandholt, S. W. H. Cowley, Y. Miyoshi, F. J. Rich, V. K. Jordanova, R. B. Torbert, and A. Sharma (2007),

The magnetosphere under weak solar wind forcing, *Ann. Geophys.*, *25*, 191–205.

Fear, R. C., S. E. Milan, A. N. Fazakerley, E. A. Lucek, S. W. H. Cowley, and I. Dandouras (2008), The azimuthal extent of three flux transfer events, *Ann. Geophys.*, *26*, 2353–2369.

Greenwald, R. A., et al. (1995), Darn/SuperDarn: A global view of the dynamics of high-latitude convection, *Space Sci. Rev.*, *71*, 761–796, doi:10.1007/BF00751350.

Grocott, A., S. W. H. Cowley, and J. B. Sigwarth (2003), Ionospheric flow during extended intervals of northward but B_Y-dominated IMF, *Ann. Geophys.*, *21*, 509–538.

Grocott, A., S. V. Badman, S. W. H. Cowley, T. K. Yeoman, and P. Cripps (2004), The influence of IMF By on the nature of the nightside high-latitude ionospheric flow during intervals of positive IMF Bz, *Ann. Geophys.*, *22*, 1755–1764.

Grocott, A., S. E. Milan, and T. K. Yeoman (2008), Interplanetary magnetic field control of fast azimuthal flows in the nightside high-latitude ionosphere, *Geophys. Res. Lett.*, *35*, L08102, doi:10.1029/2008GL033545.

Hill, T. W. (1979), Inertial limit on corotation, *J. Geophys. Res.*, *84*, 6554–6558.

Hill, T. W., A. J. Dessler, and C. K. Goertz (1983), Magnetospheric models, in *Physics of the Jovian Magnetosphere*, edited by A. J. Dessler, pp. 353–394, Cambridge Univ. Press, New York.

Hubert, B., S. E. Milan, A. Grocott, C. Blockx, S. W. H. Cowley, and J.-C. Gérard (2006), Dayside and nightside reconnection rates inferred from IMAGE FUV and Super Dual Auroral Radar Network data, *J. Geophys. Res.*, *111*(A10), A03217, doi:10.1029/2005JA011140.

Jackman, C. M., N. Achilleos, E. J. Bunce, S. W. H. Cowley, M. K. Dougherty, G. H. Jones, S. E. Milan, and E. J. Smith (2004), Interplanetary magnetic field at ~9 AU during the declining phase of the solar cycle and its implications for Saturn's magnetospheric dynamics, *J. Geophys. Res.*, *109*(A18), A11203, doi:10.1029/2004JA010614.

Kamide, Y., and A. D. Richmond (1982), Ionospheric conductivity dependence of electric fields and currents estimated from ground magnetic observations, *J. Geophys. Res.*, *87*, 8331–8337.

Kan, J. R., and L. C. Lee (1979), Energy coupling function and solar wind-magnetosphere dynamo, *Geophys. Res. Lett.*, *6*, 577–580.

Khan, H., and S. W. H. Cowley (1999), Observations of the response time of high-latitude ionospheric convection to variations in the interplanetary magnetic field using EISCAT and IMP-8 data, *Ann. Geophys.*, *17*, 1306–1335, doi:10.1007/s005850050858.

Khurana, K. K. (2001), Influence of solar wind on Jupiter's magnetosphere deduced from currents in the equatorial plane, *J. Geophys. Res.*, *106*, 25,999–26,016.

Kuo, H., C. T. Russell, and G. Le (1995), Statistical studies of flux transfer events, *J. Geophys. Res.*, *100*, 3513–3519.

Mayaud, P. N. (1980), *Derivation, Meaning, and Use of Geomagnetic Indices*, *Geophys. Monogr. Ser.*, vol. 22, AGU, Washington, D. C.

McAndrews, H. J., C. J. Owen, M. F. Thomsen, B. Lavraud, A. J. Coates, M. K. Dougherty, and D. T. Young (2008), Evidence for reconnection at Saturn's magnetopause, *J. Geophys. Res.*, *113*(A12), A04210, doi:10.1029/2007JA012581.

McComas, D. J., S. J. Bame, P. Barker, W. C. Feldman, J. L. Phillips, P. Riley, and J. W. Griffee (1998), Solar Wind Electron Proton Alpha Monitor (SWEPAM) for the advanced composition explorer, *Space Sci. Rev.*, *86*, 563–612, doi:10.1023/A:1005040232597.

Milan, S. (2004), Dayside and nightside contributions to the cross polar cap potential: Placing an upper limit on a viscous-like interaction, *Ann. Geophys.*, *22*, 3771–3777.

Milan, S. E., G. Provan, and B. Hubert (2007), Magnetic flux transport in the Dungey cycle: A survey of dayside and nightside reconnection rates, *J. Geophys. Res.*, *112*(A1), A01209, doi:10.1029/2006JA011642.

Newbury, J. A., C. T. Russell, J. L. Phillips, and S. P. Gary (1998), Electron temperature in the ambient solar wind: Typical properties and a lower bound at 1 AU, *J. Geophys. Res.*, *103*, 9553–9566.

Nichols, J. D., S. W. H. Cowley, and D. J. McComas (2006), Magnetopause reconnection rate estimates for Jupiter's magnetosphere based on interplanetary measurements at ~5 AU, *Ann. Geophys.*, *24*, 393–406.

Perreault, P., and S.-I. Akasofu (1978), A study of geomagnetic storms, *Geophys. J. Int.*, *54*, 547–573, doi:10.1111/j.1365-246X.1978.tb05494.x.

Rostoker, G., and C.-G. Fälthammar (1967), Relationship between changes in the interplanetary magnetic field and variations in the magnetic field at the Earth's surface, *J. Geophys. Res.*, *72*, 5853–5863.

Ruohoniemi, J. M., and K. B. Baker (1998), Large-scale imaging of high-latitude convection with Super Dual Auroral Radar Network HF radar observations, *J. Geophys. Res.*, *103*, 20,797–20,811.

Ruohoniemi, J. M., and R. A. Greenwald (1996), Statistical patterns of high-latitude convection obtained from Goose Bay HF radar observations, *J. Geophys. Res.*, *101*, 21,743–21,763.

Russell, C. T., R. P. Lepping, and C. W. Smith (1990), Upstream waves at Uranus, *J. Geophys. Res.*, *95*, 2273–2279.

Russell, C. T., G. Le, and H. Kuo (1996), The occurrence rate of flux transfer events, *Adv. Space Res.*, *18*, 197–205, doi:10.1016/0273-1177(95)00965-5.

Russell, C. T., J. G. Luhmann, and G. Lu (2001), Nonlinear response of the polar ionosphere to large values of the interplanetary electric field, *J. Geophys. Res.*, *106*, 18,495–18,504.

Russell, C. T., C. M. Jackman, H. Y. Wei, C. Bertucci, and M. K. Dougherty (2008), Titan's influence on Saturnian substorm occurrence, *Geophys. Res. Lett.*, *35*, L12105, doi:10.1029/2008GL034080.

Scurry, L., and C. T. Russell (1991), Proxy studies of energy transfer to the magnetosphere, *J. Geophys. Res.*, *96*, 9541–9548.

Shepherd, S. G., J. M. Ruohoniemi, and R. A. Greenwald (2003), Testing the Hill model of transpolar potential with Super Dual Auroral Radar Network observations, *Geophys. Res. Lett.*, *30*(1), 1002, doi:10.1029/2002GL015426.

Siscoe, G. L., and D. Summers (1981), Centrifugally driven diffusion of Iogenic plasma, *J. Geophys. Res.*, *86*, 8471–8479.

Smith, C. W., J. L'Heureux, N. F. Ness, M. H. Acuña, L. F. Burlaga, and J. Scheifele (1998), The ACE magnetic fields experiment, *Space Sci. Rev.*, *86*, 613–632, doi:10.1023/A:1005092216668.

Stone, E. C., A. M. Frandsen, R. A. Mewaldt, E. R. Christian, D. Margolies, J. F. Ormes, and F. Snow (1998), The advanced composition explorer, *Space Sci. Rev.*, *86*, 1–22, doi:10.1023/A:1005082526237.

Wang, Y. L., R. C. Elphic, B. Lavraud, M. G. G. T. Taylor, J. Birn, C. T. Russell, J. Raeder, H. Kawano, and X. X. Zhang (2006), Dependence of flux transfer events on solar wind conditions from 3 years of Cluster observations, *J. Geophys. Res.*, *111*(A10), A04224, doi:10.1029/2005JA011342.

Wygant, J. R., R. B. Torbert, and F. S. Mozer (1983), Comparison of S3-3 polar cap potential drops with the interplanetary magnetic field and models of magnetopause reconnection, *J. Geophys. Res.*, *88*, 5727–5735.

S. V. Badman, S. W. H. Cowley, A. Grocott, S. E. Milan, J. D. Nichols, and T. K. Yeoman, Department of Physics and Astronomy, University of Leicester, University Road, Leicester LE1 7RH, UK. (a.grocott@ion.le.ac.uk)